universe

MDPI

Article

Corrections on the Distribution of Nuclei Due to Neutron Degeneracy and Its Effect on R-Process in Neutron Star Black Hole Mergers

Rita K. Y. Lau

HKU SPACE Po Leung Kok Stanley Ho Community College, 66 Leighton Road, Causeway Bay, Hong Kong; kityulau.rita@gmail.com

Abstract: The r-process is one of the processes that produces heavy elements in the Universe. One of its possible astrophysical sites is the neutron star–black hole (NS-BH) merger. We first show that the neutrons can degenerate before and during the r-process in these mergers. Previous studies assumed neutrons were non-degenerate and the related rates were calculated under Maxwell–Boltzmann approximations. Hence, we corrected the related rates with neutron degeneracy put in the network code and calculated with the trajectories of NS-BH mergers. We show that there are differences in the nuclei distributions. The heating rates and the temperature at most can be two times larger. The change in heating rates and temperature can affect the light curves of the kilonovae. However, this has little effect on the final abundances.

Keywords: nuclear astrophysics; nuclear reactions; r-process; neutron stars; black holes

check for updates

Citation: Lau, R.K.Y. Corrections on the Distribution of Nuclei Due to Neutron Degeneracy and Its Effect on R-Process in Neutron Star Black Hole Mergers. *Universe* **2024**, *10*, 401. https://doi.org/10.3390/universe10100401

Academic Editor: Daniela D. Doneva

Received: 30 July 2024
Revised: 25 September 2024
Accepted: 12 October 2024
Published: 18 October 2024

1. Introduction

R-process is one of the processes that produces heavy elements in the Universe. Burbidge et al. [1], Cowan et al. [2], Thielemann et al. [3]. One of the sites of the process was just confirmed recently. The observations of gravitational waves due to a merger of two neutron stars (NS-NS) and the kilonovae afterward have confirmed that the r-process occurred in these merging systems Arcavi et al. [4], Pian et al. [5], Abbott et al. [6], Smartt et al. [7], Valenti et al. [8], Cowperthwaite et al. [9]. After that, the gravitational waves produced by the merging of a neutron star with a black hole (NS-BH) have also been observed. Abbott et al. [10], Broekgaarden et al. [11]. It is believed that this merging system can also be a potential site for the r-process. Surman et al. [12], Goriley et al. [13], Rosswog et al. [14], Wanajo et al. [15], Rosswog et al. [16], Foucart [17], Siegel [18]. Similar to NS-NS mergers, the observations of the light curves of the mergers between NS-BHs are also expected [19–22]. Some of the kilonovae (blue kilonova and red kilonova) are nuclear-origin [19]. The luminosity depends on the nuclear heating rates as well as the temperatures.

It was already shown that the neutrons degenerate in the inner crusts of the neutron stars [23] and corrections of the degenerate neutron capture rates were evaluated [24,25]. The correction of the degeneracy [24] on the neutron capture rates was also implemented in the neutron star crusts codes [23] and it was discovered that the nuclei shifted to more neutron-rich sides. We proposed that similar situations also occurred in neutron star–black hole mergers.

Simulations of merging systems were carried out much earlier than their observations. A network calculation of NS mergers was first conducted in Freiburghaus et al. [26]. The network calculations of NS-NS and NS-BH mergers were further studied in Surman et al. [12], Goriley et al. [13], Rosswog et al. [14], Wanajo et al. [15], Rosswog et al. [16]. At the beginning of merging, the temperature was so high that the neutron capture rates and the inverse photodisintegration rates can be assumed to be at equilibrium. We called it nuclear statistical equilibrium (NSE). This is typical in network calculations of the r-process. Surman et al. [12], Goriley et al. [13], Rosswog et al. [14], Wanajo et al. [15], Rosswog et al. [16]. It is no surprise

that neutrons degenerate in this situation due to high densities. Moreover, in this paper we will show that neutrons can also degenerate after NSE. Actually, degeneracy also plays a role during the r-process. Saha equations were typically used to calculate the distribution of nuclei during NSE. However, the typical Saha equations assumed neutrons are Maxwell–Boltzmann distributions but at such a high density the neutrons degenerate. Furthermore, neutron capture rates and photodisintegration rates without neutron degeneracy corrections Cyburt et al. [27,28] were also used during the r-process. In this paper, we modify the Saha equations with neutron degeneracy by a correction factor. We also correct the distribution of nuclei after NSE by a correction factor. We will show how the correction factor can be calculated in Section 2.

This paper is organized as follows. First, we discuss the NS-BH trajectories used in the r-process simulations Rosswog et al. [14], Piran et al. [29], Korobkin et al. [30]. Next, we talk about the nuclear data used and how the Saha equation due to neutron degeneracy is corrected by using a correction factor. We argued that we can approximate the distribution of nuclei after NSE by the same correction factor. In Section 3, we show that the neutrons can degenerate during the r-process and study how this affects the heating rates and hence the temperature during the NSE and r-process. The effects on the final abundances of the r-process will also be briefly discussed. At the end, we present some conclusions.

2. Methods

2.1. Trajectories of NS-BH Mergers

In this paper, we study the situation of NS-BH mergers. The trajectories presented in Rosswog et al. [14], Piran et al. [29], Korobkin et al. [30] are used. We investigate a black hole of 10 solar masses merging with a 1.4 solar mass neutron star with 4.93×10^{-10} solar mass ejected. A high mass for the black hole was chosen to maximize the effects of neutron degeneracy in the merging system. There were in total, 20 different trajectories with various electron abundances, referred to as case 1 for trajectory-ns14-BH10-irrot-1-checked.dat, case2 for trajectory-ns14-BH10-irrot-2-checked.dat, and so on. The trajectories without self-heating are from the literature mentioned above. The nuclear reaction network (Skynet as we will mention later) also includes the heat energy generated by nuclear reactions. Figure 1 shows the temperature and densities (without and with self-heating) of Case 16 (Ye = 8.07×10^{-2}). Case 16 is chosen as neutron degeneracy has large effects on the temperatures and heating rates as well as distribution of nuclei.

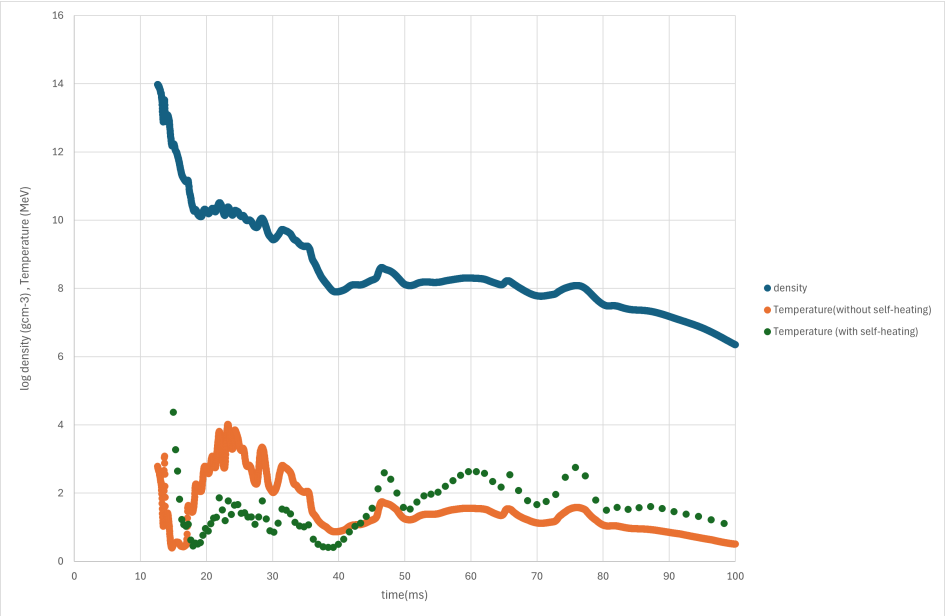

Figure 1. Temperature and density versus time for Case 16 without and with self heating.

2.2. Degeneracy Factor and Neutron Fermi Energy

Next, we use a degeneracy factor to decide whether the neutrons in the ejecta of the merger degenerate or not. The degeneracy factor is defined as the neutron chemical energy divided by the energy of the temperature:

$$degeneracy\ factor = \mu_n / kT, \tag{1}$$

where μ_n is the chemical potential of the neutron, k is Boltzmann's constant, and T is the temperature. We define the degeneracy factor larger than 1 as neutron degenerate. In Section 3, we will show that the neutrons degenerate at the beginning as well as during the r-process. In reality, μ_n (the neutron chemical potential) depends on the equation of the state of the neutron star. For simplicity, we approximated the neutrons as a Fermi gas. We assume the neutron chemical potential is equal to the Fermi energy of a non-interacting Fermi gas which is

$$E_f = \frac{\hbar^2}{2m}(3\pi^2 N/V)^{2/3} \tag{2}$$

where $\hbar$ is Planck's constant, E_F is the Fermi energy of the neutrons, m is the mass of the neutron, and $\frac{N}{V}$ is the number density.

Actually, we can expect that the interacting neutrons will increase the neutron chemical potential and increase the degeneracy effects. The neutron chemical potential heavily depends on the equation of states (EOS). But the investigation of the issue is out of the scope of the present paper.

Figure 2 shows the degeneracy factor versus time for Case 16. Case 16 is chosen again as it has large effects on the results. We can see that the degeneracy factor, in general, decreases with time. This is expected as the neutrons should be less degenerate with an increase in time due to the expansion of the ejecta and hence decrease in density. From the figure we can see that the degeneracy factor drops below 1 roughly at 0.02 s. It implies that the neutrons degenerate before 0.02 s.

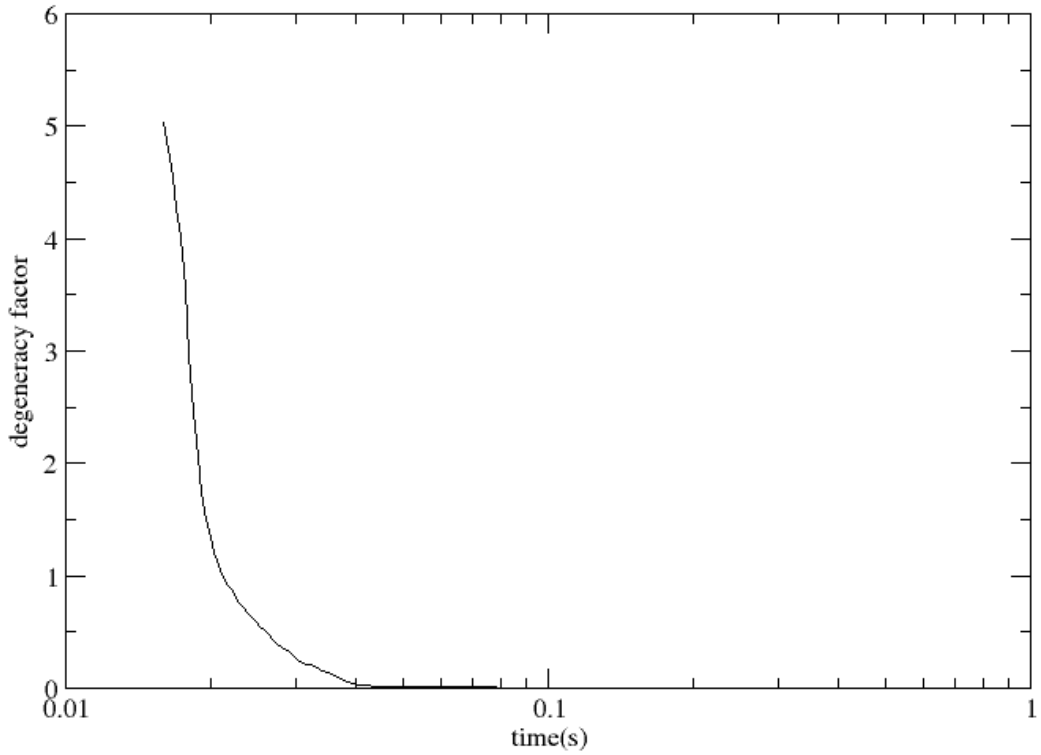

Figure 2. Degeneracy factor versus time for case 16.

2.3. SkyNet

The code SkyNet Lippuner and Roberts [31] was used to perform the calculations of the nuclear reactions in the ejecta of a merger. For the beta decay rates, we used the Fuller and Fowler (FFNU) rates Fuller [32], Langanke and Martinez-Pindo [33]. For the theoretical partition function, we used the WINVN file [34]. We included fission in the SkyNet Panov et al. [35,36] but neutrino reactions were not included.

At the beginning of the merger, the neutron capture rates were so high that the time steps had to be made too small for the tracking. NSE was assumed. The Saha equations were used to calculate the NSE.

The Saha equation for an ideal Maxwell–Boltzmann gas is [37]

$$\frac{n_{A+1}}{n_A n_n} = 1/2 \frac{e^{Q/kT}(2J_{A+1}+1)(A+1)^{3/2}}{(2J_A+1)(A)^{3/2}} \left(\frac{m_n k_B T}{2\pi\hbar^2}\right)^{-3/2}. \tag{3}$$

where n_A is the number density of nuclei A, n_{A+1} is the number density of nuclei $A+1$, n_n is the number density of neutrons, J is the spin, m_n is the mass of neutron, k_B is Boltzmann's constant, T is the temperature, $\hbar$ is Planck's constant, and Q is the neutron separation energy

The present paper studies the effects of neutron degeneracy on the r-process. Thus, the Saha requires modification. The Saha equations using the neutron degeneracy corrections to a Fermi–Dirac distribution can be found in Lau [38]. Here, we repeat that derivation.

First, we can approximate the nuclei other than neutrons as a Maxwell–Boltzmann gas due to their small abundances. The typical highest abundances of the nuclei are around 1.0×10^{-4} and the nuclei have larger atomic masses, typically in the order of 100 times that of the neutron. Thus, it is valid to assume the nuclei other than the neutrons are a Maxwell–Boltzmann gas. For an ideal Maxwell–Boltzmann gas,

$$n_A = \frac{(2J_A+1)(2\pi m_A k_B T)^{3/2}}{h^3} e^{\mu/k_B T} \tag{4}$$

where n_A is the number density of nuclei A, n_{A+1} is the number density of nuclei $A+1$, J is the spin, m is the mass, k_B is Boltzmann's constant, T is the temperature, $\hbar$ is Planck's constant, and μ is the chemical potential; while

$$n_{A+1} = \frac{(2J_{A+1}+1)(2\pi m_{A+1} k_B T)^{3/2}}{h^3} e^{\mu_{A+1}/k_B T}. \tag{5}$$

We assume neutron capture and photodisintegration rates are at equilibrium of a single isotope here because the rates are much faster than the beta decay rates due to the high temperatures in such a merger. This is not a bad assumption. In equilibrium, the chemical potential is

$$\mu_A + m_A c^2 + \mu_n + m_n c^2 = \mu_{A+1} + m_{A+1} c^2. \tag{6}$$

The $Q-value$ can be written as follows:

$$Q = m_A c^2 + m_n c^2 - m_{A+1} c^2 \tag{7}$$

Combining the above equations, the corrected Saha equation (directly using the neutron densities) is

$$\frac{n_{A+1}}{n_A n_n} = \frac{(2J_{A+1}+1)(A+1)^{3/2} e^{Q/kT} exp(\mu_n/k_B T)}{(2J_A+1)(A)^{3/2} n_n}. \tag{8}$$

Thus, the correction factor is f:

$$f = 2\frac{e^{\mu_n/(k_B T)}(2\pi\hbar^2)^{-3/2}}{(m_n k_B T)^{-3/2} n_n}. \quad (9)$$

If we assume it is Fermi gas, combining Equation (2),

$$f = 3/4\pi^{1/2} e^{(\mu_n)/(k_B T)}(\mu_n/k_B T)^{-3/2} \quad (10)$$

Figure 3 shows the correction factor versus neutron chemical potential. We can see that for larger neutron chemical potential and hence the higher neutron density, the correction factor increases almost linearly.

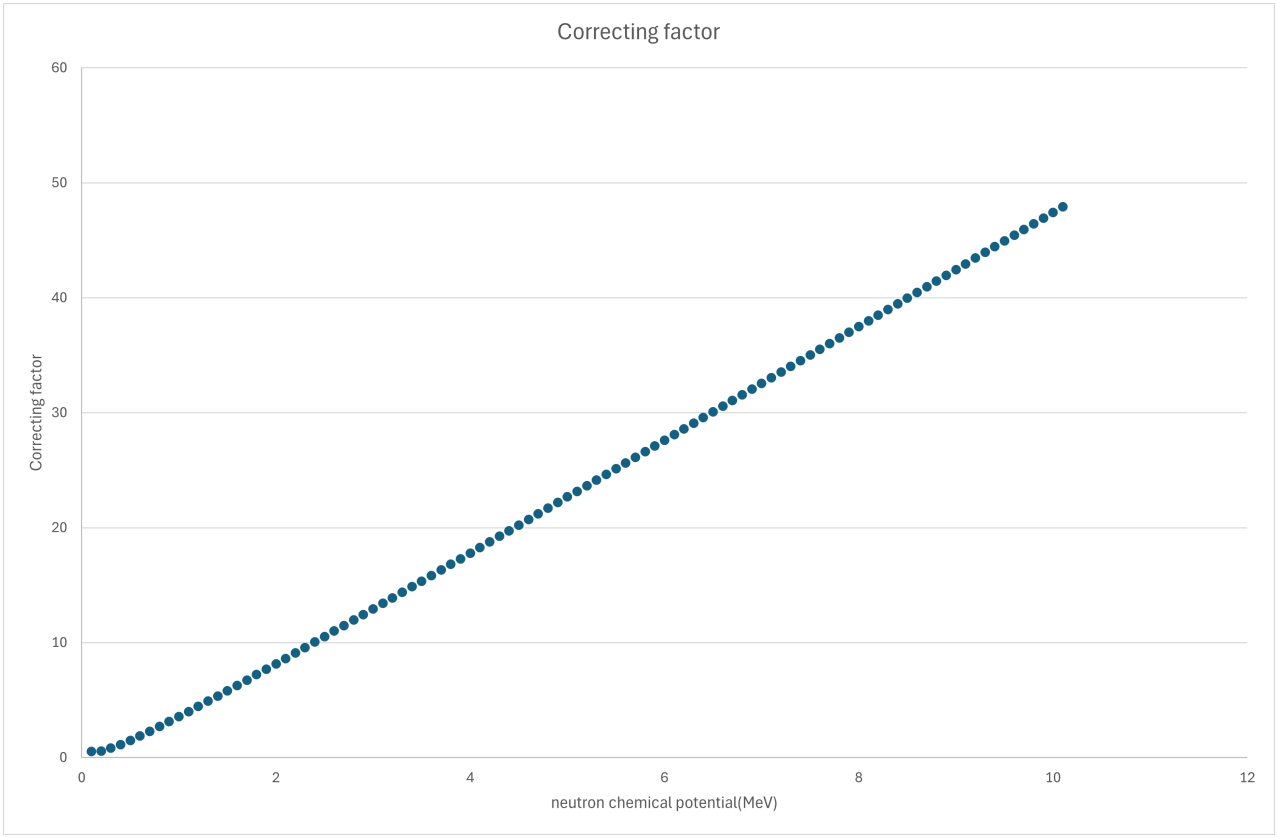

Figure 3. Correction factor versus neutron chemical potential.

Equation (10) in our paper is exactly equal to the Equation (10) in [24] which is the limiting case (strongly degenerate neutrons) for degenerate neutron capture rates. The correction factor is in between 1 to infinity. If the neutron densities are low (the neutron chemical potential is small), the correction factor will be very close to 1. If the neutron chemical potential is large, the correction factor will be extremely large which implies that neutron capture rates will be large.

The simplest way to modify the original SkyNet code (which uses the typical Saha equations) is simply directly multiplying the formula in the NSE subroutine in the code by the correction factor f.

After NSE, the Skynet code calculates the nuclear reactions using the following formula:

$$\frac{dY_i}{dt} = \sum N^i_j \lambda_j Y_j + N^i_{j,k} \rho N_A < \sigma v >_{j,k} Y_j Y_k + N^i_{j,k,l} \rho N_A < \sigma v >_{j,k,l} Y_j Y_k Y_l, \quad (11)$$

where Y_i is the abundance of isotope i, N is the number of isotopes, λ_i is the rate of the one-body reaction, $< \sigma\nu >_{i,j}$ are the rates of the two-body reactions, $< \sigma\nu >_{i,j,k}$ are the rates of the three-body reactions, N_A is Avogadro's number, and ρ is the density.

For the nuclear physics input, we implemented the JINA REACLIB from Cyburt et al. [27] but with a correction factor for the neutron capture rates. We only modified the neutron capture rates by the following arguments.

For reactions involving photons, we find the overall reaction rate $0 + 1 < - > \gamma + 3$

$$r = N_0 N_1 < \sigma v >_{01->\gamma 3} - \lambda_\gamma(3) N_3, \tag{12}$$

where r is the net rate, N is the number of isotopes, λ is the photo-disintegration rate, and $< \sigma v >$ is the two-body reaction. We assume the neutron capture and photo-disintegration rates are not too far away from equilibrium at high temperatures and high densities when the degeneracy factor is larger than 1 (See Figures 2 and 3). Thus, r is roughly zero. We can approximate the distribution of the nuclei again by the Saha equation and the correction factor is the same. However, in the code, there is no Saha equation after NSE. Thus, we need to modify the rates. The distribution of the nuclei can be represented by the following equations:

$$\frac{N_3}{N_0 N_1} = \frac{< \sigma v >_{01->\gamma 3}}{\lambda_\gamma(3)} \tag{13}$$

$$= \frac{(2J_{A+1} + 1)(A+1)^{3/2} e^{Q/kT} exp(\mu_n / k_B T)}{(2J_A + 1)(A)^{3/2} n_n} \tag{14}$$

Thus, the distribution of the nuclei is equivalent to the ratio of neutron capture rates to photodisintegration rates. Multiplying the correction factor to the neutron capture rates (or dividing the photodisintegration rate by the factor) can represent the change in the distribution of nuclei due to neutron degeneracy. This approximation in the Lau thesis [38] obtained similar results in [23] with exact rates [24]. We believe that it is a good approximation. Furthermore, as we showed before, our correction factor is just the limiting case of the exact [24] rate.

2.4. Procedure

We first included the correction factor f in the NSE subroutine in SkyNet and picked out the abundances (other than those for neutrons) and directly multiplied the abundance equations in the NSE subroutine by the correction factor and then let the subroutine conduct the iterations. Thus, the iterations will find the neutron abundances and chemical potentials which fulfill the Saha equations. The NSE subroutine outputs the initial abundances in the merger.

For the initial conditions, we chose a density that is below 1.00×10^{13} gcm $^{-3}$ and temperature higher than 1 GK but lower than 10 GK in order to fulfill the NSE condition. The smallest times which satisfy both conditions were chosen.

We also implemented the correction factor in the neutron capture rates inside the code. Since we want to study the distribution of the nuclei, only the ratio of the neutron capture rates to the photodisintegration rates is our interest. Either multiplying the neutron capture rates with the correction factor or dividing the photodisintegration rates with the same factor gives the same result. Thus, we picked out the neutron capture rates and multiplied them by the correction factor before they entered the matrix solver to calculate the abundance.

For a degeneracy factor smaller than 1, we stop multiplying by it within the code because the approximation only holds for high neutron degeneracy.

Finally, in order to see if our results are reliable, we studied all the situations with different values of mass deviation thresholds $10^{-8}, 10^{-10}$ as well as 10^{-12} to check the numerical convergence. We found that they have no observable effect on the results.

3. Results

3.1. Neutron Degeneracy in the R-Process

First, we show that neutrons can degenerate during the r-process in NS-BH mergers. In general, the neutrons degenerate all the time before the degeneracy factor reaches 1.

Table 1 shows the time, temperature, density, and electron abundance at the start of the r-process for each case. We defined the beginning of the r-process as the point of the start of the building up of the nuclei in the second peak of the solar abundances (Appendix A).

Table 2 shows the time, temperature, densities and electron abundances when the degeneracy factor reaches 1. We can see the r-process started before the degeneracy factor reached 1 for all cases except for case 5. This shows that neutrons can degenerate during the r-process.

Table 1. Time, temperature, densities and electron abundances when r-process starts, for 20 different neutron star–black hole trajectories.

Case	Time (ms)	Temperature (GK)	Densitiy (gcm^{-3})	Ye
BH10-1	13.4	9.15×10^{-1}	8.37×10^{10}	1.65×10^{-2}
BH10-2	13.0	1.66×10^{0}	5.39×10^{11}	1.66×10^{-2}
BH10-3	13.0	4.95×10^{-1}	7.67×10^{10}	2.00×10^{-2}
BH10-4	13.8	7.81×10^{-1}	1.58×10^{11}	1.18×10^{-2}
BH10-5	20.4	1.22×10^{0}	1.74×10^{10}	6.70×10^{-2}
BH10-6	15.0	7.92×10^{-1}	1.69×10^{11}	4.70×10^{-2}
BH10-7	14.6	6.68×10^{-1}	1.18×10^{11}	4.11×10^{-2}
BH10-8	12.0	1.07×10^{0}	2.02×10^{11}	9.70×10^{-2}
BH10-9	13.3	8.23×10^{-1}	1.78×10^{11}	2.20×10^{-2}
BH10-10	11.9	3.74×10^{-1}	3.45×10^{10}	1.15×10^{-1}
BH10-11	13.5	1.32×10^{0}	3.93×10^{11}	1.15×10^{-1}
BH10-12	13.4	1.35×10^{0}	3.52×10^{11}	2.35×10^{-2}
BH10-13	13.2	8.08×10^{-1}	1.61×10^{11}	1.80×10^{-2}
BH10-14	14.3	1.12×10^{0}	3.06×10^{11}	3.50×10^{-2}
BH10-15	13.6	1.31×10^{0}	3.80×10^{11}	3.10×10^{-2}
BH10-16	18.0	6.02×10^{-1}	4.19×10^{10}	8.80×10^{-2}
BH10-17	11.7	1.26×10^{0}	4.32×10^{11}	9.80×10^{-2}
BH10-18	13.3	8.20×10^{-1}	1.80×10^{11}	1.60×10^{-2}
BH10-19	12.8	7.15×10^{-1}	1.43×10^{11}	1.80×10^{-2}
BH10-20	12.9	7.57×10^{-1}	1.59×10^{11}	2.21×10^{-2}

Table 2. Time, temperature, densities and electron abundances when degeneracy factor reaches 1 for different NS-BH trajectories.

Case	Time (ms)	Temperature (GK)	Densitiy (gcm^{-3})	Ye
BH10-1	17.3	1.01×10^{-1}	1.7×10^{9}	1.65×10^{-2}
BH10-2	22.8	1.00×10^{-1}	4.8×10^{8}	1.77×10^{-2}
BH10-4	23.8	3.33×10^{-1}	2.82×10^{9}	1.91×10^{-2}
BH10-5	19.2	9.30×10^{-1}	4.60×10^{11}	6.60×10^{-2}
BH10-6	22.0	3.33×10^{-1}	2.82×10^{9}	4.92×10^{-2}
BH10-7	22.4	2.13×10^{-1}	1.40×10^{9}	4.27×10^{-2}
BH10-8	13.7	4.57×10^{-1}	3.64×10^{9}	9.53×10^{-2}
BH10-9	21.1	1.33×10^{-1}	6.94×10^{8}	2.33×10^{-2}
BH10-10	12.6	3.54×10^{-1}	2.08×10^{9}	1.10×10^{-1}
BH10-11	23.0	9.47×10^{-2}	7.14×10^{8}	1.63×10^{-2}
BH10-12	21.9	1.32×10^{-1}	6.75×10^{8}	2.35×10^{-2}
BH10-13	19.8	8.94×10^{-2}	4.00×10^{8}	1.93×10^{-2}
BH10-14	23.3	2.00×10^{-2}	1.17×10^{9}	3.73×10^{-2}
BH10-15	21.5	1.80×10^{-1}	1.03×10^{9}	3.02×10^{-2}
BH10-16	22.4	1.30×10^{0}	2.24×10^{10}	8.07×10^{-2}
BH10-17	13.6	3.98×10^{-1}	1.00×10^{10}	9.84×10^{-2}
BH10-18	22.8	9.70×10^{-1}	4.51×10^{8}	1.72×10^{-2}
BH10-19	19.1	8.72×10^{-2}	3.75×10^{8}	1.89×10^{-2}
BH10-20	19.5	1.05×10^{-1}	4.65×10^{8}	2.22×10^{-2}

3.2. Heating Effects on Temperature Changes

After running 20 trajectories with and without neutron degeneracy correction but with self-heating, we discovered that such a correction can have big effects on the heating in the r-process and hence the temperatures in some cases. In order to check the validity of our result, we quantitatively estimated the heating rates by using the dominant nuclei at 17 ms (See Appendix A). The analytical result agrees well with Figure 4 (the heating rate per gram versus time) at 17 ms.

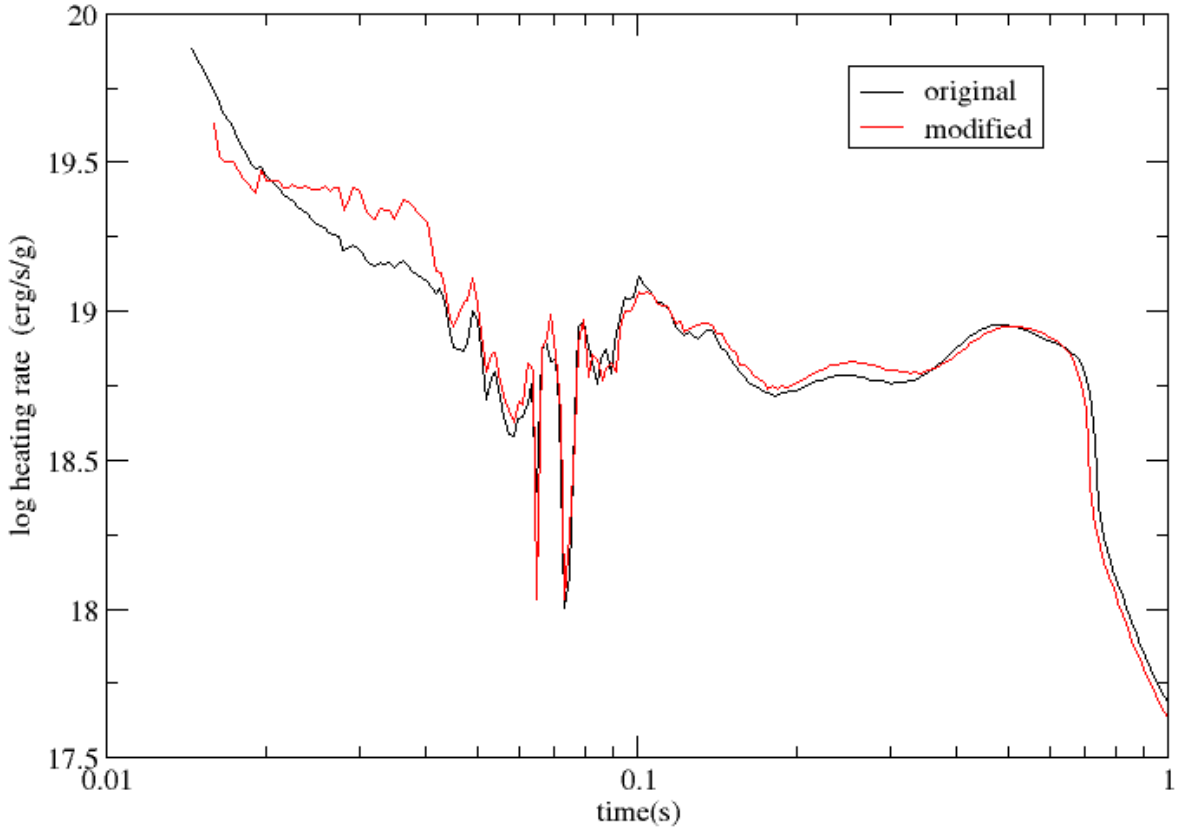

Figure 4. Heating rate versus time for case 16.

Furthermore, we integrate the absolute difference in heating rate erg/g/s with time for every case and shown it in the Table 3. We discovered that some of the cases (such as Case 16) have large values which implied that the degeneracy has great effects on the heating rate per mass. Case 5 has the largest value in Table 3. However, neutron degeneracy has great effects in NSE but no effect during the r-process in this case. Still, it can have effects on the heating rates even if the degeneracy is gone.

Table 3. The absolute integrated heat per gram for different NS-BH trajectories.

Case	Heat per Gram (ergs/g)
BH10-1	4.31×10^{15}
BH10-2	4.12×10^{16}
BH10-3	4.57×10^{15}
BH10-4	2.74×10^{16}
BH10-5	4.99×10^{17}
BH10-6	3.15×10^{16}
BH10-7	6.44×10^{16}
BH10-8	2.70×10^{17}
BH10-9	1.67×10^{16}
BH10-10	4.42×10^{17}

Table 3. *Cont.*

Case	Heat per Gram (ergs/g)
BH10-11	7.63×10^{16}
BH10-12	4.50×10^{16}
BH10-13	5.01×10^{16}
BH10-14	1.08×10^{17}
BH10-15	2.36×10^{16}
BH10-16	4.47×10^{17}
BH10-17	2.24×10^{17}
BH10-18	4.08×10^{16}
BH10-19	5.47×10^{16}
BH10-20	4.65×10^{16}

From Figures 4–6, we can see the heating rates, temperatures, and electron abundances versus time. In the beginning, from Figures 7 and 8, we can see degenerate neutron capture rates shift more nuclei to the neutron-rich sides (see Equation (1)), as well as the value of the degenerate Ye being smaller than that of the non-degenerate Ye (become more neutron-rich which is consistent to shifting nuclei to the neutron-rich side), leading a decrease in energy due to the negative $Q - values$ of the neutron capture rates for neutron-rich nuclei and hence lower heating rate. Later on (after 22 ms when the degeneracy effect was gone), due to the higher mass of the nuclei produced, the beta decay neutron emissions rates for high masses are much higher than those for the low masses; the heating rates increase (at most two times) and hence lead to increases (at most two times) in temperature (one can see that for Ye it is higher in the presence of degeneracy than in the absence of degeneracy which is again consistent as beta decay shift nuclei have higher Ye value). One of the remarkable things is that there are also differences in the heat produced after the degeneracy effect is gone (0.02 s). After 0.1 s, the effects due to neutron degeneracy are completely gone. Figures 7–9 show the abundance plots, which are the distribution of the nuclei (with and without neutron degeneracy correction) for different times. The abundance plot without neutron degeneracy correction at 17 ms was shown in Figure 10 in the previous subsection. The heat rates and the temperature can affect the light curves of the kilonovae. However, the detailed investigation is out of the scope of the paper.

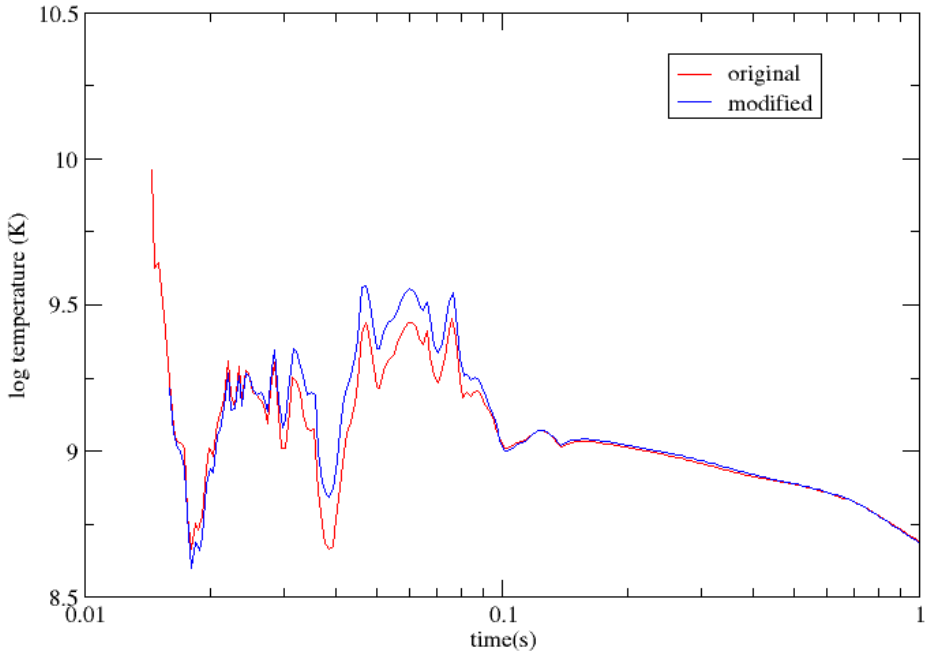

Figure 5. Temperature versus time for case 16.

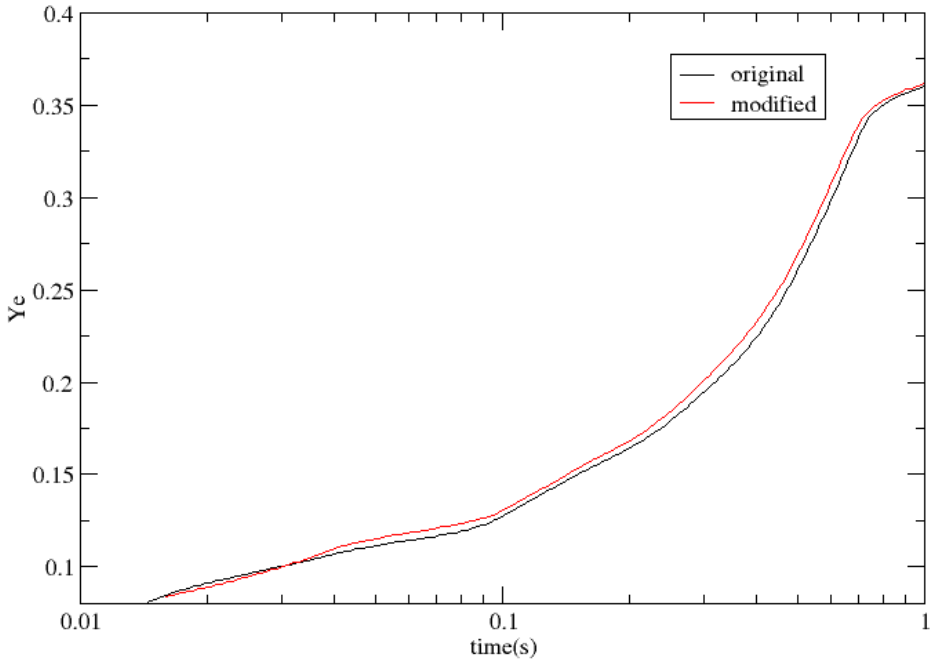

Figure 6. Electron abundance versus time for Case 16.

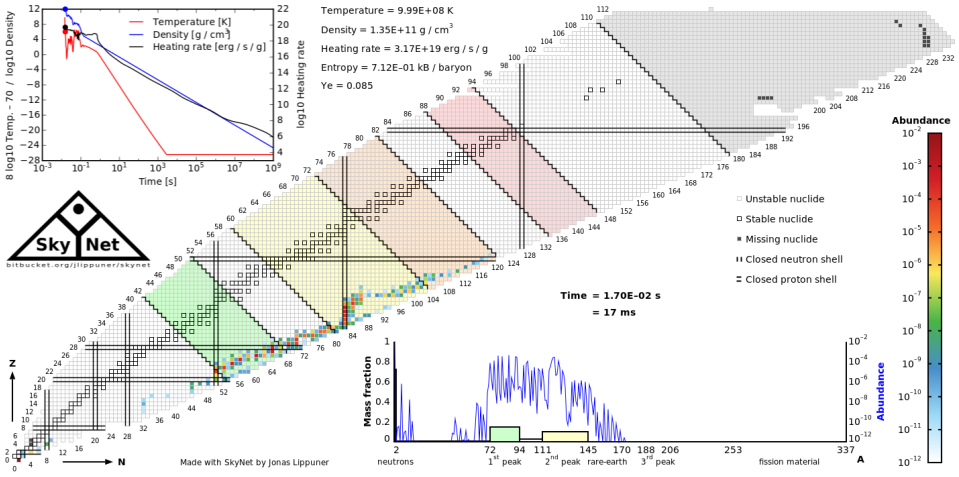

Figure 7. Initial situation for Case 16 with neutron degeneracy correction.

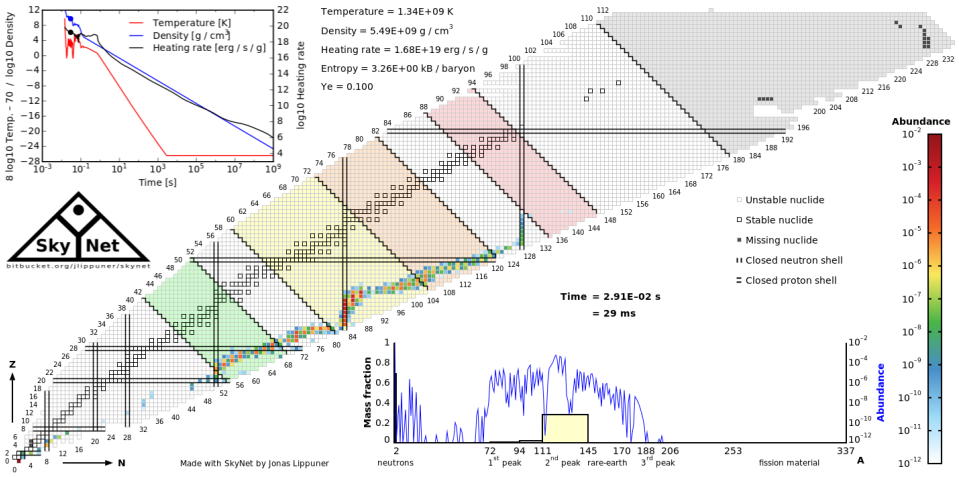

Figure 8. Case 16 without neutron degeneracy correction at 30 ms.

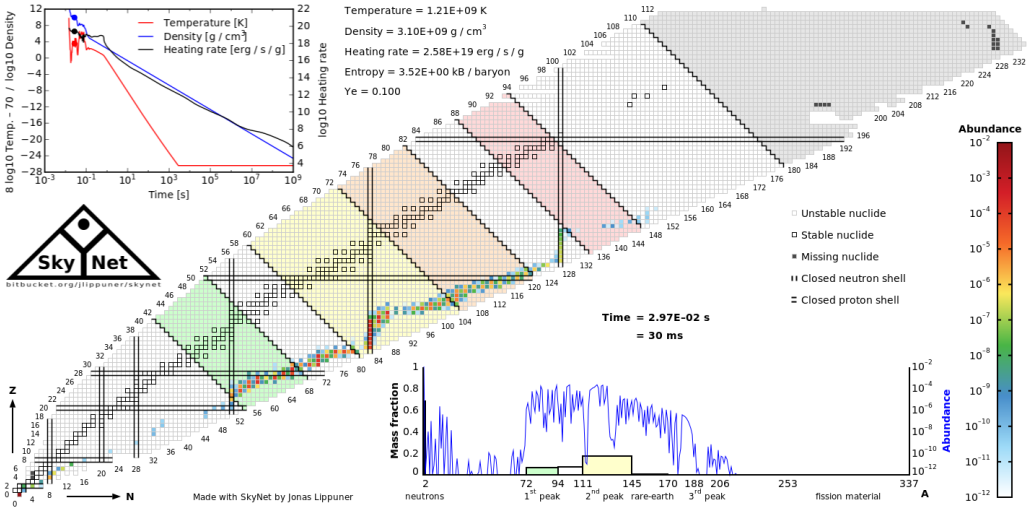

Figure 9. Case 16 with neutron degeneracy correction at 30 ms.

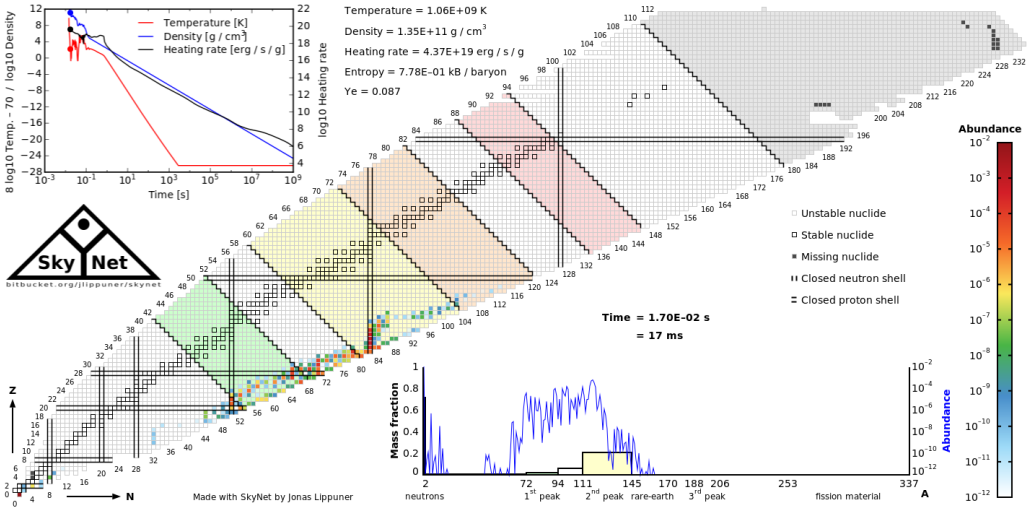

Figure 10. Abundance plot when the r-process starts (without correction).

3.3. Final Abundances

Comparing the final abundances with and without neutron degeneracy, we find that there is not much difference. This is expected, as the degenerate neutron capture rates happen in the early stages of the r-process and the effects are washed out by later nuclear reactions and hence have little effect on the final abundances. Figure 11 shows one of the cases (Case 16). We can see that both of the cases (with and without neutron degeneracy) reproduced the typical r-process abundances.

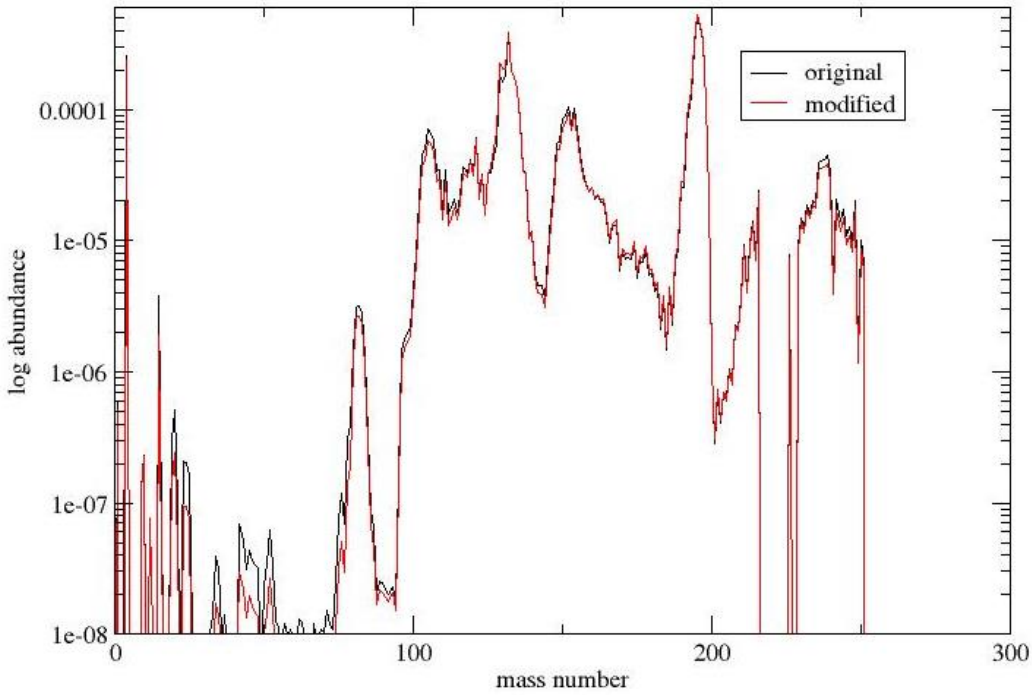

Figure 11. Final abundances versus mass number for Case 16.

4. Discussion

The trajectories of NS-BH mergers were used to study the effects on the production of heavy elements in the r-process in Rosswog et al. [14,16], Piran et al. [29], Korobkin et al. [30]. They examined different trajectories and concluded that the final abundances produced are kind of consistent with the solar abundances. We reach the same conclusion as well. The final abundances can reproduce the features of the solar abundances (see Section 3).

From Section 3, we can see that the consideration of neutron degeneracy mostly increases the temperatures of the system. The detailed impacts due to the degeneracy of the light curves can be further investigated which is out of the scope of the paper.

The beta-delayed neutron emission rates may also decrease as the neutron emissions may be blocked due to the high Fermi energy of the neutron. These reactions may lead to further changes in the final abundance and the heat generation of the r-process. However, a set of consistent rates with a neutron degeneracy correction is not presently available. Thus, we leave it to be conducted in future projects.

Actually, the neutron chemical potential should be higher than the Fermi energy, as the neutrons should have interactions. The effects of the light curves actually may even be stronger.

Furthermore, neutron degeneracy may also need to be taken into account in the r-processes in other scenarios, such as NS-NS mergers and hypernovae, possibly revising the final abundances and heat generation.

5. Conclusions

In this paper, we first showed that neutrons can degenerate in the ejecta at the beginning as well as during the r-process in the NS-BH mergers. This neutron degeneracy has effects on the distribution of the nuclei and roughly at most two times in the heating rates. The temperature can be at most two times larger. This can affect the light curve. However, this has little effect on the final abundance. Neutron degeneracy can also affect the other nuclear reaction types in the r-process such as beta-delayed neutron emissions during the r-process. This may also further affect the final abundances as well as heat generation in the r-process. Moreover, neutron star mergers and hypernovae may also have neutron degeneracy effects. This issue should be further studied.

Funding: This research received no external funding.

Data Availability Statement: The raw data supporting the conclusions of this article will be made available by the authors on request.

Acknowledgments: The author wants to thank Hendrik Schatz and Otto Tang for discussions of the project.

Conflicts of Interest: The author declares no conflicts of interest. The funders had no role in the design of the study; in the collection, analyses, or interpretation of data; in the writing of the manuscript; or in the decision to publish the results.

Appendix A

Here, we estimate the change of the heating rate quantitatively due to the degenerate neutron capture rates. We used the time 17 ms for Case 16 as shown in the paper (Figure 4). For simplicity, we picked up abundant nuclei at time ^{111}As with neutron capture rate 2.65×10^{-4} cm^{-3}mol^{-1}s^{-1} (from JINA REACLIB) and the Q value which is -0.564 MeV (from JINA REACLIB). The temperature at 17 ms is around 1 GK with density 1.34×10^{11} gcm^{-3}. The difference in neutron abundance is 0.001 (See Figures 7 and 10 for the Ye). Thus, the heating rate is -0.564 MeV $\times$ 1.60×10^{-6} ergs/MeV $\times$ 1.34×10^{11} gcm^{-3} $\times$ 2.65×10^{-4} cm^{3}mol^{-1}s^{-1} $\times$ 6.02×10^{23}/111 mole/g $= 1.75 \times 10^{19}$ erg/s/g which the order of magnitude is consistent with the graph (Figure 4) of the difference in the heating rate at 17 ms.

References

1. Burbidge, E.M.; Burbidge, G.R.; Fowler, W.A.; Hoyle, F. Synthesis of the elements in stars. *Rev. Mod. Phy.* **1957**, *29*, 547–650. [CrossRef]
2. Cowan, J.; Thielemann, F.K.; Truran, J.W. The r-process and nucleochronology. *Phys. Rep.* **1991**, *208*, 267–394. [CrossRef]
3. Thielemann, F.; Arcones, A.; Käppeli, F.; Liebendörfer, M. Rauscher, T.; Winteler, C.; Fröhlich, C.; Dillmann, I.; Fischer, T.; Martinez-Pinedo, G.; et al. What are the astrophysical sites for the r-process and the production of heavy elements? *Prog. Part. Nucl. Phys.* **2011**, *66*, 346–353. [CrossRef]
4. Arcavi, I.; Hosseinzadeh, G.; Howell, D.A.; McCully, C.; Poznanski, D.; Kasen, D.; Barnes, J.; Zaltzman, M.; Vasylyev, S.; Maoz, D.; et al. Optical emission from a kilonova following a gravitational-wave-detected neutron-star merger. *Nature* **2017**, *551*, 64–66. [CrossRef]
5. Pian, E.; D'Avanzo, P.; Benetti, S.; Branchesi, M.; Brocato, E.; Campana, S.; Cappellaro, E.; Covino, S.; D'Elia, V.; Fynbo, J.P.U.; et al. Spectroscopic identification of r-process nucleosynthesis in a double neutron-star merger. *Nature* **2017**, *551*, 67–70. [CrossRef] [PubMed]
6. Abbott, B.; Abbott, R.; Abbott, T.D.; Acernese, F.; Ackley, K.; Adams, C.; Adams, T.; Addesso, P.; Adhikari, R.X.; Adya, V.B.; et al. GW170817: Observation of Gravitational Waves from a Binary Neutron Star Inspiral. *Phys. Rev. Lett.* **2017**, *119*. [CrossRef]
7. Smartt, S.J.; Chen, T.-W.; Jerkstrand, A.; Coughlin, M.; Kankare, E.; Sim, S.A.; Fraser, M.; Inserra, C.; Maguire, K.; Chambers, K.C.; et al. A kilonova as the electromagnetic counterpart to a gravitational-wave source. *Nature* **2017**, *551*, 75–79. [CrossRef]
8. Valenti, S.; David, J.; Yang, S.; Cappellaro, E.; Tartaglia, L.; Corsi, A.; Jha, S.W.; Reichart, D.E.; Haislip, J.; Kouprianov, V. The discovery of the electromagnetic counterpart of GW170817: Kilonova AT 2017gfo/DLT17ck. *Astrophys. J. Lett.* **2017**, *848*, L24. [CrossRef]
9. Cowperthwaite, P.S.; Berger, E.; Villar, V.A.; Metzger, B.D.; Nicholl, M.; Chornock, R.; Blanchard, P.K.; Fong, W.; Margutti, R.; Soares-Santos, M. The electromagnetic counterpart of the binary neutron star merger LIGO/Virgo GW170817. II. UV, optical, and near-infrared light curves and comparison to kilonova. *Astrophys. J. Lett.* **2017**, *848*, L17. [CrossRef]
10. Abbott, R.; Abbott, T.D.; Abraham, S.; Acernese, F.; Ackley, K.; Adams, A.; Adams, C.; Adhikari, R.X.; Adya, V.B.; Affeldt, C.; et al. GWTC-2: Compact Binary Coalescences Observed by LIGO and Virgo during the First Half of the Third Observing Run. *Phys. Rev. X* **2021**, *11*, 021053.
11. Broekgaarden, F.S.; Berger, E.; Neijssel, C.J.; Vigna-Gómez, A.; Chattopadhyay, D.; Stevenson, S.; Chruslinska, M.; Justham, S.; de Mink, S.E.; Mandel, I. Impact of massive binary star and cosmic evolution on gravitational wave observations I: Black hole–neutron star mergers. *Mon. Not. R. Astron. Soc.* **2021**, *508*, 4. [CrossRef]
12. Surman, R.; McLaughlin, G.C.; Ruffert, M.; Janka, H.-T.; Hix, W.R. r-Process nucleosynthesis in hot accretion disk flows from black hole-neutron star mergers. *Astrophys. J.* **2008**, *679*, L117. [CrossRef]
13. Goriely, S.; Bauswein, A.; Janka, H.-T. R-process nucleosynthesis in dynamically ejected matter of neutron star mergers. *Astrophys. J. Lett.* **2011**, *738*, L32. [CrossRef]
14. Rosswog, S.; Korobkin, O.; Arcones, A.; Thielemann, F.-K.; Piran, T. The long-term evolution of neutron star merger remnants–I. The impact of r-process nucleosynthesis. *Mon. Not. R. Astron. Soc.* **2013**, *430*, 2585–2604. [CrossRef]

15. Wanajo, S.; Sekiguchi, Y.; Nishimura, N.; Kiuchi, K.; Kyutoku, K.; Shibata, M. Production of all the r-process nuclides in the dynamical ejecta of neutron star mergers. *Astrophys. J. Lett.* **2014**, *789*, L39. [CrossRef]
16. Rosswog, S.; Feindt, U.; Korobkin, O.; Wu, M.-R.; Sollerman, J.; Goobar, A.; Martinez-Pinedo, G. Detectability of compact binary merger macronovae. *Class. Quantum Gravity* **2017**, *34*, 104001. [CrossRef]
17. Foucart, F. A brief overview of black hole-neutron star mergers. *Front. Astron. Space Sci.* **2020**, *7*, 46. [CrossRef]
18. Siegel, D. r-Process nucleosynthesis in gravitational-wave and other explosive astrophysical events. *Nat. Rev. Phys.* **2022**, *4*, 306–318. [CrossRef]
19. Barbieri, C.; Salafia, O.S.; Perego, A.; Colpiand, M.; Ghirlanda, G. Light-curve models of black hole–neutron star mergers: Steps towards a multi-messenger parameter estimation. *Astron. Astrophys.* **2019**, *625*, A152. [CrossRef]
20. Ackley, K.; Amati, L.; Barbieri, C.; Bauer, F.E.; Benetti, S.; Bernardini, M.G.; Bhirombhakdi, K.; Botticella, M.T.; Branchesi1, M.; Brocato, E.; et al. Observational constraints on the optical and near-infrared emission from the neutron star–black hole binary merger candidate S190814bv. *Astron. Astrophys.* **2020**, *643*, A113. [CrossRef]
21. Barbieri, C.; Salafia, O.S.; Perego, A.; Colpi, M.; Ghirlanda, G. Electromagnetic counterparts of black hole–neutron star mergers: dependence on the neutron star properties. *Eur. Phys. J. A* **2020**, *56*, 8. [CrossRef]
22. Anand, S.; Coughlin, M.W.; Kasliwal, M.M.; Bulla, M.; Ahumada, T.; Carracedo, A.S.; Almualla, M.; Andreoni, I.; Stein, R.; Foucart, F.; et al. Optical follow-up of the neutron star–black hole mergers S200105ae and S200115j. *Nat. Astron.* **2021**, *5*, 46–53. [CrossRef]
23. Lau, R.; Beard, M.; Gupta, S.S.; Schatz, H.; Afanasjev, A.V.; Brown, E.F.; Deibel, A.L.; Gasques, R.; Hitt, G.W.; Hix, W.R. Nuclear reactions in the crusts of accreting neutron stars. *Astrophys. J.* **2018**, *859*, 62. [CrossRef]
24. Shternin, P.S.; Beard, M.; Wiescher, M.; Yakovlev, D.G. Neutron degeneracy and plasma physics effects on radiative neutron captures in neutron star crust. *Phy. Rev. C* **2012**, *86*, 015808. [CrossRef]
25. Knight, B.; Caballero, L. Computing Neutron Capture Rates in Neutron-Degenerate Matter. *Universe* **2019**, *5*, 36. [CrossRef]
26. Freiburghaus, C.; Rembges, J.-F.; Rauscher, T.; Kolbe, E.; Thielemann, F.-K.; Kratz, K.-L.; Pfeiffer, B.; Cowan, J.J. The astrophysical r-process: A comparison of calculations following adiabatic expansion with classical calculations based on neutron densities and temperatures. *Astrophys. J.* **1999**, *525*, L121. [CrossRef]
27. Cyburt, R.H.; Amthor, A.M.; Ferguson, R.; Meisel, Z.; Smith, K.; Warren, S.; Heger, A.; Hoffman, R.D.; Rauscher, T.; Sakharuk, A. The JINA REACLIB database: Its recent updates and impact on type-I X-ray bursts. *Astrophys. J. Suppl.* **2010**, *189*, 240. [CrossRef]
28. Cyburt, R.H.; Amthor, A.M.; Heger, A.; Johnson, E.; Keek, L.; Meisel, Z.; Schatz1, H.; Smith, K. Dependence of X-ray burst models on nuclear reaction rates. *Astrophys. J.* **2016**, *830*, 55. [CrossRef]
29. Piran, T.; Nakar, E.; Rosswog, S. The electromagnetic signals of compact binary mergers. *Mon. Not. R. Astron. Soc.* **2013**, *430*, 2121–2136. [CrossRef]
30. Korobkin, O.; Rosswog, S.; Arcones, A.; Winteler, C. On the astrophysical robustness of the neutron star merger r-process. *Mon. Not. R. Astron. Soc.* **2012**, *426*, 1940–1949. [CrossRef]
31. Lippuner, J.; Roberts, L.R. SkyNet: A modular nuclear reaction network library. *Astrophys. J. Suppl.* **2017**, *233*, 18. [CrossRef]
32. Fuller, G.M.; Fowler, W. Stellar Weak Interaction Rates1 for Intermediate Mass Nuclei. III. Rate Tables for the Free Nucleons and Nuclei with ^{4} = 21 TO ^{4} = 60. *Astrophys. J. Suppl.* **1982**, *48*, 279–320. [CrossRef]
33. Langanke, K.; Martinez-Pindo, G. Rate tables for the weak processes of pf-shell nuclei in stellar environments. *At. Data Nucl. Data Tables* **2001**, *79*, 1–46. [CrossRef]
34. Rauscher, T. Evolution and nucleosynthesis of massive stars and related nuclear uncertainties. *Astrophys. J. Suppl.* **2003**, *233*, 403. [CrossRef]
35. Panov, I.V.; Korneev, I.Y.; Rauscher, T.; Martínez-Pinedo, G.; Kelić-Heil, A.; Zinner, N.T.; Thielemann, F.-K. Neutron-induced astrophysical reaction rates for translead nuclei. *Astron. Lett.* **1995**, *21*, A61. [CrossRef]
36. Panov, I.V.; Blinnikov, S.I.; Thielemann, F.-K. Nucleosynthesis of heavy elements: Computational experiment. *Astron. Lett.* **2001**, *27*, 239–248. [CrossRef]
37. Illiadis, C. *Nuclear Physics of Stars*; Wiely: Hoboken, NJ, USA, 2007.
38. Lau, K.Y. Nuclear Reaction in the Crust of Accreting Neutron Stars. Ph.D. Thesis, Michiagn State University, East Lansing, MI, USA, 2012.